Available online at www.sciencedirect.com
SCIENCE DIRECT®
International Journal of Thermal Sciences 43 (2004) 587–593
International Journal of Thermal Sciences
www.elsevier.com/locate/ijts

Thermocapillary convection in a differentially heated annular pool for moderate Prandtl number fluid

You-Rong Li [a,*], Lan Peng [a], Shuang-Ying Wu [a], Dan-Ling Zeng [a], Nobuyuki Imaishi [b]

[a] *College of Power Engineering, Chongqing University, 400044, People's Republic of China*
[b] *Institute for Materials Chemistry and Engineering, Kyushu University, Fukuoka, Japan*

Received 9 July 2003; accepted 4 December 2003

Available online 12 February 2004

Abstract

In order to understand the nature of thermocapillary convection under microgravity in a differentially heated annular pool with the outer heated container of radius $r_o = 40$ mm and the inner cooled cylinder of $r_i = 20$ mm, and an adjustable depth $d = 3$–14 mm, we conducted a series of unsteady two-dimensional numerical simulations with the finite volume method. The pool was filled with the 0.65cSt silicone oil (Prandtl number $Pr = 6.7$). With a large enough temperature difference in the radial direction, the simulation can predict oscillatory thermocapillary flows. Hopf bifurcation neutral curve is delineated in the thermocapillary Reynolds number (Re)-aspect ratio ($A = (r_o - r_i)/d$) plane. It is found that time-dependent motion is only possible if A exceeds a critical value A_{cri} which is around 2.29. Streamline and isotherm patterns are presented at different thermocapillary Reynolds number and the aspect ratio corresponding to stationary and oscillatory states.

Keywords: Computer simulation; Fluid flow; Thermocapillary convection; Silicone oil; Annular pool

1. Introduction

Understanding fluid motion is very important in crystal growth from the melt. Generally, single crystals with uniform material properties are desired, but homogeneity in crystals can be destroyed if melt motion is unsteady [1]. In a micro-gravity environment or a shallow liquid layer, thermocapillarity is the major cause for melt convection. It is known that convection becomes oscillatory when the temperature difference along the free surface exceeds a critical value. In the past few decades, thermocapillary convection has received much attention from both fundamental and industrial aspects. Levich and Krylov [2], Ostrach [3] and Davis [4] provided good reviews on early studies. At the same time, many numerical simulations were also performed for low and high Pr fluids. Ben Hadid and Roux [5–7] considered the two-dimensional (2-D) thermocapillary and thermocapillary-buoyancy convection of fluid with low Pr number, $Pr = 0.015$, in cavities of various aspect ratios (A), and showed the existence of a multicellular steady flow, and a transition from steady to oscillatory flow when the Ma number exceeds a critical value. Villers and Platten [8] have carried out both experiments and 2-D simulations for acetone ($Pr = 4$), and have confirmed the existence of the multicellular flow. Peltier and Biringen [9] reported the results of 2-D numerical simulation of oscillatory thermocapillary convection of a fluid with moderate $Pr = 6.78$ in cavities and provided a stability diagram in the (A, Ma)-plane. They found a minimum critical A near 2.3 and a minimum critical Ma near 20 000 within the range of $A \leqslant 3.8$. Xu and Zebib [10] further performed 2-D calculations for fluids with $1 < Pr < 10$ in cavities and determined the neutral curves for the Hopf bifurcation as a function of the capillary Reynolds number and aspect ratio. On the other hand, many experiments of thermocapillary flow subjected to a horizontal temperature gradient along the upper free surface for rectangular geometries [11–18] and annular geometry [19–22] were carried out in normal gravity. The character of various 2-D and three-dimensional (3-D) thermocapillary convections was examined and the existence of thermocapillary instabilities [23] was demonstrated. Recently, Schwabe et al. [24,25] reported a successful thermocapillary convec-

* Corresponding author.
E-mail address: liyourong@yahoo.com (Y.-R. Li).

1290-0729/$ – see front matter
doi:10.1016/j.ijthermalsci.2003.12.003

Nomenclature

A	aspect ratio, $=(r_o - r_i)/d$	γ_T	temperature coefficient of surface tension ..... $N\cdot m^{-1}\cdot K^{-1}$
d	depth ..... m	μ	dynamic viscosity ..... $kg\cdot m^{-1}\cdot s^{-1}$
Ma	Marangoni number, $=\gamma_T \Delta T(r_o - r_i)/(\mu\alpha)$	ν	kinematic viscosity ..... $m^2\cdot s^{-1}$
p	pressure ..... Pa	Θ	non-dimensional temperature, $=(T - T_C)/(T_H - T_C)$
P	non-dimensional pressure, $=p/(\rho\nu^2/r_o^2)$	ρ	density of the fluid ..... $kg\cdot m^{-3}$
Pr	Prandtl number, $=\nu/\alpha$	τ	non-dimensional time
r	radius ..... m	ψ	non-dimensional stream function
R	non-dimensional radial coordinate		
Re	thermocapillary Reynolds number, $=\gamma_T \Delta T d/(\nu\mu)$	*Subscripts*	
t	time ..... s	C	cooled
T	temperature ..... K	cri	critical
$\boldsymbol{V}$	non-dimensional velocity vector	H	heated
V	non-dimensional velocity	i	inner
z	axial coordinate ..... m	o	outer
Z	non-dimensional axial coordinate	r	radial
Greek symbols		z	axial
α	thermal diffusivity ..... $m^2\cdot s^{-1}$		

tion experiment under microgravity in the Russian satellite FOTON-12. In this experiment, an annular gap with an outer heated container of radius $r_o = 40$ mm and an inner cooled cylinder of $r_i = 20$ mm, and an adjustable depth of $d = 2.5-20$ mm, was subjected to various radial temperature gradients. They observed the stationary structure of concentric multirolls for small Marangoni number, hydrothermal waves for larger *Ma*, and more complicated temperature oscillations foreven higher *Ma*. They also measured the onset of oscillations under microgravity and under normal gravity, and found a significant stabilization of thermocapillary convection by the action of gravity. In the present study, we report on results of unsteady 2-D numerical simulations to understand the nature of thermocapillary convection of a moderate *Pr* fluid in an annular pool with the same radius as Schwabe experiment subjected to a horizontal temperature gradient.

2. Physical and mathematic models

2.1. Basic assumptions and governing equations

We analyze the thermocapillary flow of the 0.65cSt silicone oil ($Pr = 6.7$) in a differentially heated annular pool of depth d, inner radius r_i and outer radius r_o, as shown schematically in Fig. 1. The bottom boundary is rigid while the top boundary is a non-deformable flat free surface open to a passive gas. Both bottom and top boundaries are assumed to be adiabatic. The inner and outer cylinders are maintained at constant temperatures T_C and T_H ($T_H > T_C$), respectively. The horizontal temperature gradient varies in the radial direction, so that the convection is generated by

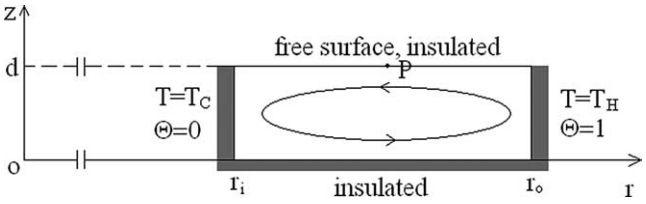

Fig. 1. Physical model.

the surface tension gradient on the top surface. The following assumptions are introduced in our model: (1) Silicone oil is an incompressible Newtonian fluid and the Boussinessq approximation is applicable except for the surface tension. (2) The velocity is small and the flow is the 2-D laminar. (3) At the top free surface, the thermocapillary force is taken into account. At other solid–liquid boundaries, the no-slip condition is applied. The problem is non-dimensionalized by using $r_o^2/\nu, r_o,\ \nu/r_o,\ (T_H - T_C)$ and $\rho\nu^2/r_o^2$ as scale quantities for time, length, velocity, temperature and pressure, respectively.

With the above assumptions, the flow and heat transfer equations are expressed in a non-dimensional form as follows.

$$\nabla \cdot \boldsymbol{V} = 0 \tag{1}$$

$$\frac{\partial \boldsymbol{V}}{\partial \tau} + \boldsymbol{V}\cdot\nabla\boldsymbol{V} = -\nabla P + \nabla^2 \boldsymbol{V} \tag{2}$$

$$\frac{\partial \Theta}{\partial \tau} + \boldsymbol{V}\cdot\nabla\Theta = \frac{1}{Pr}\nabla^2\Theta \tag{3}$$

The boundary conditions are: at the free surface ($Z = d/r_o,\ r_i/r_o < R < 1$)

$$\frac{\partial V_r}{\partial Z} = \frac{ARe}{1 - r_i/r_o}\frac{\partial \Theta}{\partial R} \tag{4a}$$

Table 1
Physical properties of silicone oil at 20 °C

ν [m^2·s^{-1}]	α [m^2·s^{-1}]	ρ [kg·m^{-3}]	γ_T [N·(mK)$^{-1}$]	Pr
0.65×10^{-6}	0.97×10^{-7}	760	-8.5×10^{-5}	6.7

$$V_z = 0 \tag{4b}$$

$$\frac{\partial \Theta}{\partial Z} = 0 \tag{4c}$$

at the bottom ($Z = 0,\ r_i/r_o < R < 1$)

$$V_r = 0 \tag{5a}$$

$$V_z = 0 \tag{5b}$$

$$\frac{\partial \Theta}{\partial Z} = 0 \tag{5c}$$

at the inner cylinder ($R = r_i/r_o,\ 0 \leqslant Z \leqslant d/r_o$)

$$V_r = 0 \tag{6a}$$

$$V_z = 0 \tag{6b}$$

$$\Theta = 0 \tag{6c}$$

at the outer cylinder ($R = 1,\ 0 \leqslant Z \leqslant d/r_o$)

$$V_r = 0 \tag{7a}$$

$$V_z = 0 \tag{7b}$$

$$\Theta = 1 \tag{7c}$$

where the nondimensional parameters: $Re = \gamma_T (T_H - T_C) d/(\mu\nu)$ and $Pr = \nu/\alpha$, are the thermocapillary Reynolds number and the Prandtl number, respectively. The thermophysical properties of silicone oil at 20 °C are listed in Table 1.

The velocity field is displayed in terms of the nondimensional stream function Ψ, which is defined as

$$V_r = -\frac{1}{R}\frac{\partial \psi}{\partial Z}, \qquad V_z = \frac{1}{R}\frac{\partial \psi}{\partial R} \tag{8}$$

This definition results in positive value of ψ for a clockwise flow and negative for counter-clockwise flow.

2.2. Numerical method

The fundamental equations are discretized by the finite volume method. The central difference approximation is applied to the diffusion terms while the second order upwind scheme is used for the convective terms. The HSMAC algorithm is used to correct simultaneously the pressure and the velocities. In this study, non-uniform staggered grids of $62^r \times (22-42)^z$ are used. In order to check the grid convergence, simulations with three set different meshes, as shown in Table 2, are performed for the liquid layer of $d = 3$ mm at $\Delta T = 2$ K. These three sets of grids produced similar flow patterns and oscillation characteristics. However, the frequency of temperature oscillation at the free surface monitoring point P ($r = 30$ mm) showed small grid dependence. Therefore, the meshes selected in this study are sufficient for accurate simulation. For other depths, sufficient grid convergence was confirmed as well for each mesh. Validation of the code for the thermocapillary flow simulation was carefully done by comparing our simulation solutions with the experimental results in Refs. [24,25]. Details of comparison are provided in Section 3.3. The non-dimensional time increment was chosen between 10^{-6} and 4×10^{-6}, which corresponds approximately to $(2-8) \times 10^{-3}$ seconds. The convergence at each time step was assumed if the maximum non-dimensional residual error of the continuity equation among all control volumes became less than 10^{-7}.

Table 2
Mesh dependence

Mesh	$52^r \times 16^z$	$62^r \times 22^z$	$72^r \times 32^z$
Frequency [Hz]	0.058122	0.058594	0.058608

3. Results and discussion

3.1. Stability diagram

In order to determine the Hopf bifurcation neutral curve, a series of numerical simulations has been conducted for the annular pool depths d from 3 mm to 14 mm (corresponding to aspect ratio $A = (r_o - r_i)/d$ from 6.67 to 1.43) and the temperature differences along the free surface from 0.5 K to 20 K. Fig. 2 shows the stability diagram and the experimental results [24,25]. It is found that there exists a critical aspect ratio $A_{\text{cri}} = 2.29$, below which the flow is stable in the considered range of thermocapillary Reynolds number. Because the real flow is the 3-D flow, this 2-D simulation predicts the low first critical Reynolds number.

When the aspect ratio A exceeds the critical value, there exists an unstable region bounded by two different critical Reynolds numbers, i.e., as Re goes up, the flow first changes from steady to oscillatory at Re_{cri1}, and then becomes stable again when Re_{cri2} is reached. Re_{cri2} grows monotonically

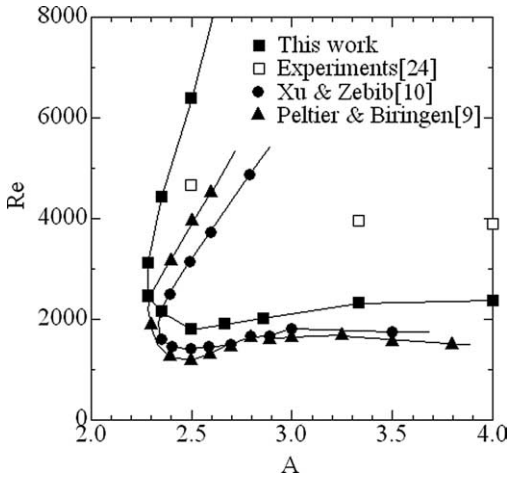

Fig. 2. Stability diagram.

with A while Re_{cri1} does not. We compare critical Reynolds numbers in the annular pools with these obtained by Peltier and Biringen [9] and Xu and Zebib [10] in cavities. It is found that the first critical value in the annular pool is slightly higher than that in cavities, but the second critical value goes up much quickly comparing with the results in cavities, as shown in Fig. 2.

3.2. Steady thermocapillary flow

A set of typical simulation streamlines and isotherms for steady thermocapillary convection is presented in Fig. 3(a). When the depth exceeds 5 mm, the flow field is unicellular with rapid inward flow from the hot outer cylinder to the cold inner cylinder along the free surface and a return flow towards the outside near the bottom. On the contrary, a small second co-rotating roll cell appears in fluid layers of $d \leqslant 4$ mm and the strength of the second co-rotating roll cell increases as the temperature difference along the free surface. Convection due to the flow cell motion causes thin thermal boundary layers near the inner and outer cylinders. Large temperature drops occur across those boundary layers so that the effective temperature gradient near the center of the annulus is lower than the imposed temperature gradient. With increasing of the depth, the thermal boundary layers become much more important. When $d > 6$ mm, it can be found that there is almost no temperature drop in the middle of the annular pool, all the temperature drop takes place in the vertical boundary layers. The simulated surface temperature and velocity distributions are shown in Fig. 3(b) and (c), respectively, for the cases of $d = 3$, 7 and 11 mm at $\Delta T = 1$ K. Because of the thin thermal boundary layer, the surface temperature exhibits a large radial temperature gradient in the region close to the inner and outer cylinders, and, as a result, the surface velocity is relatively large in these regions. For all depths, the maximum radial velocity appears on the free surface and near the inner cylinder. Because of the large surface velocity, it is found that the interior becomes cooler than the free surface just above. That means the thermal stratification is evident. The vertical temperature profiles depend mainly on the depth of liquid layer. For small depth, the vertical temperature gradient is large and almost uniform along z direction. When depth

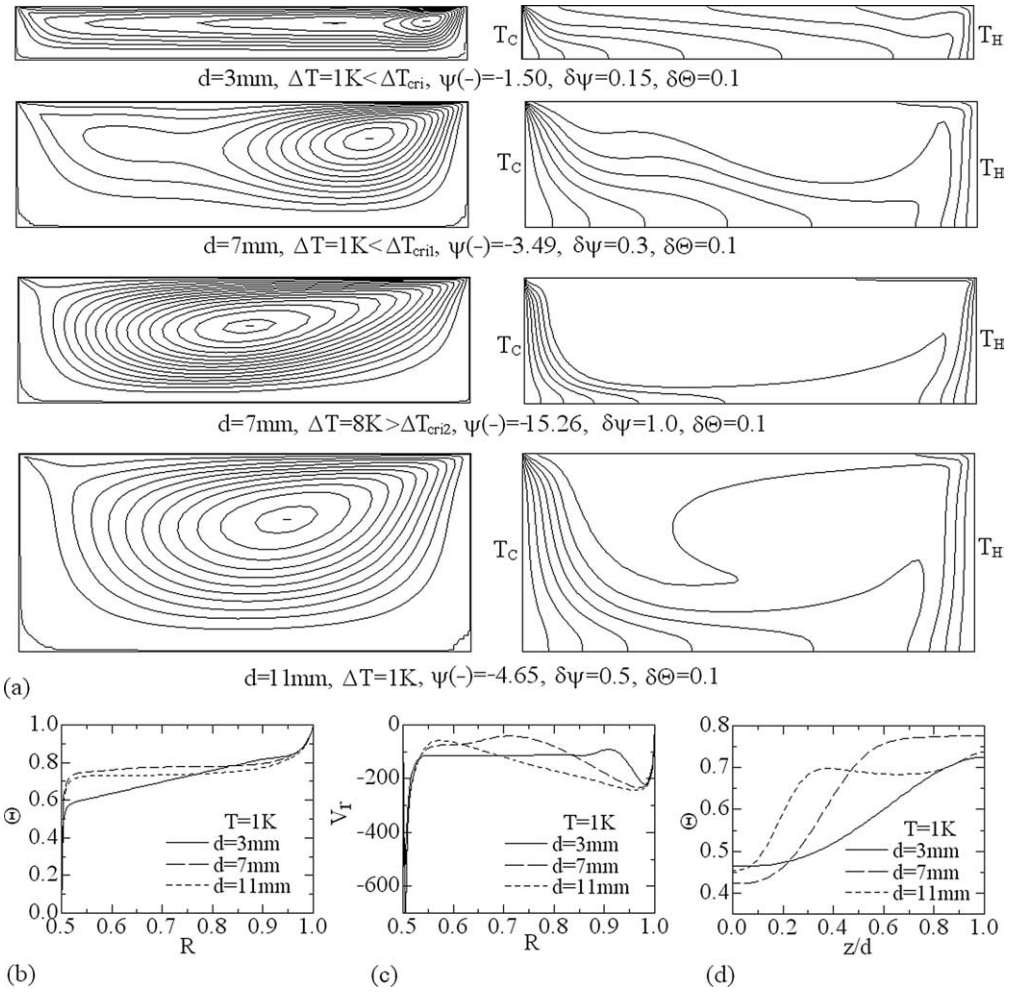

Fig. 3. Steady thermocapillary flow. (a) Streamlines and isotherms. (b) Distribution of surface temperature. (c) Distribution of surface radial velocity. (d) Temperature profiles as a function of z at $R = 0.75$.

increases, this gradient increases near the bottom, where the thermal boundary layers are formed. However, it becomes almost zero in $0.35 < z/d < 0.8$, even, an inversion of the vertical gradient can be observed in this region when $d \geqslant 9$ mm, as shown in Fig. 3(d).

3.3. Oscillatory thermocapillary flow

When the aspect ratio exceeds the critical value, for example, $A = 6.67$ ($d = 3$ mm), the flow cell near the hot cylinder is strengthened with the increase in temperature difference ΔT. Further increase in ΔT to the first critical point, which is around 1.8 K, causes the thermocapillary convection to oscillate very weakly. When ΔT exceeds the first critical point, oscillatory thermocapillary convection appears. Fig. 4(a) and (b) show the snapshots of streamlines and isotherms at four instances at $\Delta T = 2$ and 6 K, respectively. When $\Delta T = 2$ K, the flow cells originate near the inner cylinder, travel along the radial direction and merge into the stable strong cell near the outer cylinder. These moving cells are similar with the hydrothermal wave reported by Smith and Davis [23] from linear stability analysis. When ΔT increases, for example, $\Delta T = 6$ K, the strong cell near the hot cylinder becomes unstable. In

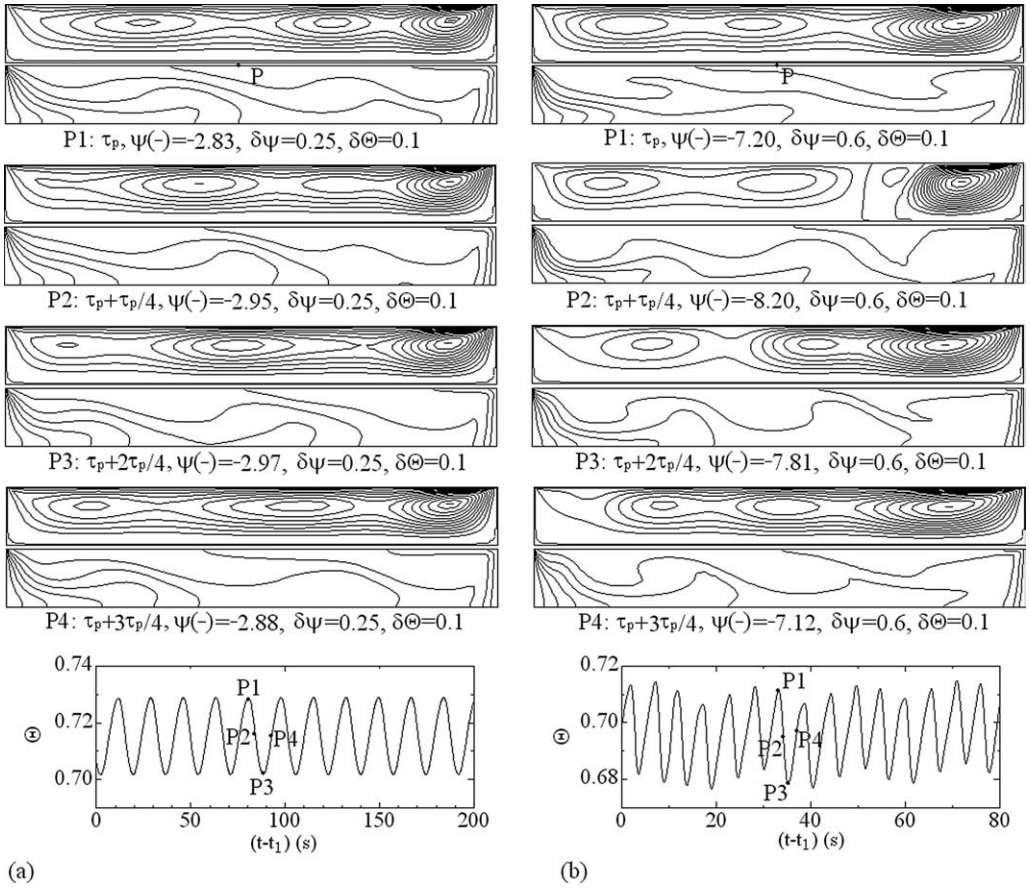

Fig. 4. Snapshots of streamlines and isotherms at four instances and temperature fluctuations at the monitoring point P for the liquid layer of $d = 3$ mm. (a) $\Delta T = 2$ K. (b) $\Delta T = 6$ K.

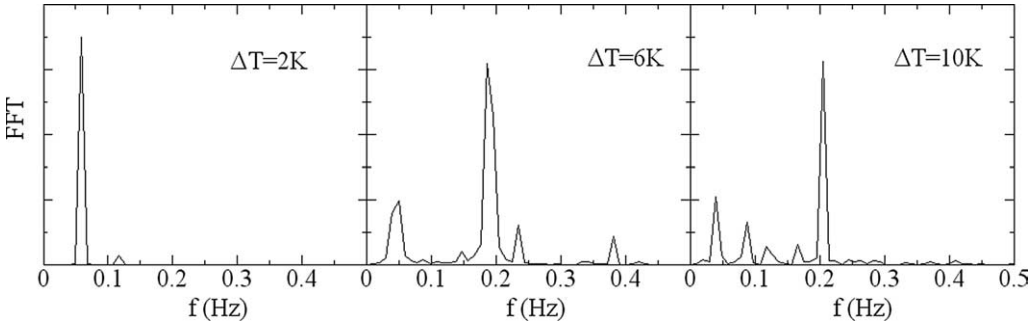

Fig. 5. Fourier spectra of temperature fluctuations at the monitoring point P for the liquid layers of $d = 3$ mm.

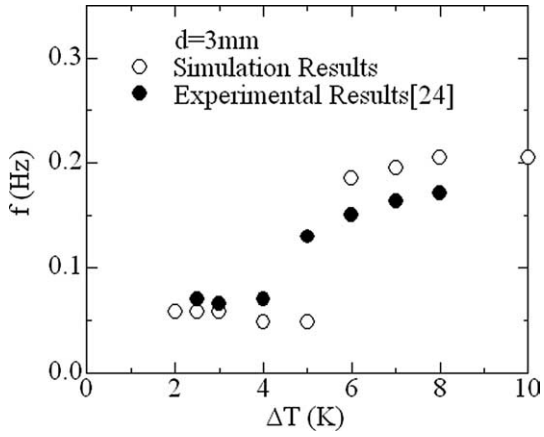

Fig. 6. Frequency of local surface temperature oscillations at the monitoring point P.

this case, the strong cell extends and contracts along the radial direction, which makes temperature fluctuations at the monitoring point P to become more and more complicated, as shown in Fig. 4(b). The frequency of the flow cells moving is different from that of the strong cell extending and contracting. Fig. 5 gives the results of Fourier spectra of temperature fluctuations at the monitoring point P for the liquid layers of $d = 3$ mm. Obviously, single frequency is obtained for the small temperature difference ΔT, but many frequency peaks appear at increased ΔT. Fig. 6 shows the main frequency of local surface temperature oscillations at the monitoring point P as a function of temperature difference ΔT for $d = 3$ mm. Obviously, the main frequency jumps when ΔT exceeds about 5 K. This trend is similar with the experimental results of Schwabe and Benz [24,25] and the 3-D simulation results [26]. Furthermore, compared Fig. 4 and Fig. 10 in Ref. [26], it is found that the 2-D and 3-D simulations predicted the similar flow pattern and oscillatory characteristics. Therefore, the 2-D simulation results can help us greatly in understanding the oscillatory flow mechanism.

With the increasing of the depth, the number of the moving cells decreases. When the depth exceeds 6 mm, there exists only one strong cell near the hot cylinder. Fig. 7 shows snapshots of streamlines and isotherms at six instances at $\Delta T = 2$ K and $d = 7$ mm. When the strong cell extends along the radial direction, it occupies the empty pool and intensity decreases. But when it contracts toward the hot cylinder, intensity increases and another small counter-clockwise is formed near the cold cylinder which results in the more complicated temperature fluctuations at the monitoring point P.

Schwabe and Benz [25] reported the measured period of oscillations as a function of pool depth under a constant ΔT. Fig. 8 shows the simulated frequency periods and the experimental results [25] at different liquid depths for a constant value of $\Delta T = 3$ K. The agreement is fairly good for the shallow layers, but the present simulations could not

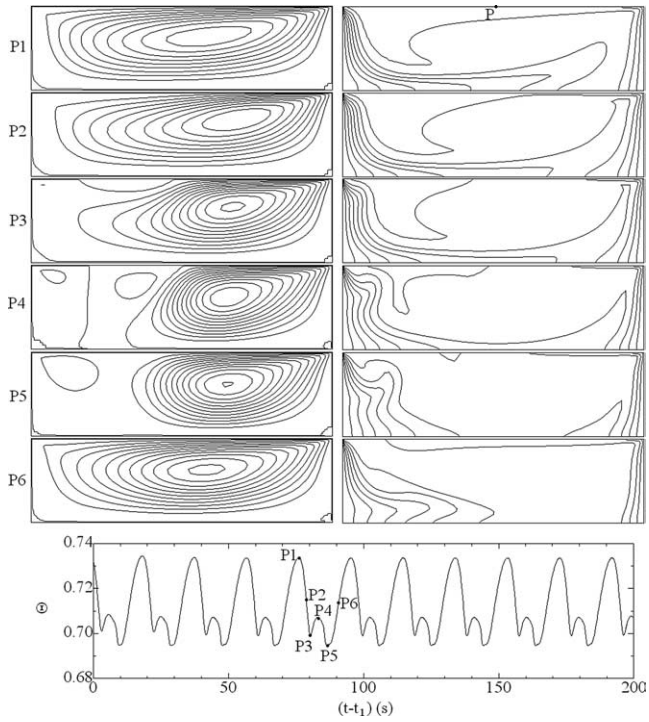

Fig. 7. Snapshots of streamlines and isotherms at four instances and temperature fluctuations at the monitoring point P for the liquid layer of $d = 7$ mm. (P1) τ_0, $\psi(-) = -9.73$, $\delta\psi = 1.0$, $\delta\Theta = 0.1$; (P2) $\tau_0 + \tau_p/6$, $\psi(-) = -9.94$, $\delta\psi = 1.0$, $\delta\Theta = 0.1$; (P3) $\tau_0 + 2\tau_p/6$, $\psi(-) = -11.24$, $\psi(+) = 0.33, \delta\psi = 1.0$, $\delta\Theta = 0.1$; (P4) $\tau_0 + 3\tau_p/6$, $\psi(-) = -11.80$, $\psi(+) = 1.43$, $\delta\psi = 1.0, \delta\Theta = 0.1$; (P5) $\tau_0 + 4\tau_p/6$, $\psi(-) = -12.07$, $\delta\psi = 1.0$, $\delta\Theta = 0.1$; (P6) $\tau_0 + 5\tau_p/6$, $\psi(-) = -11.31$, $\delta\psi = 1.0$, $\delta\Theta = 0.1$.

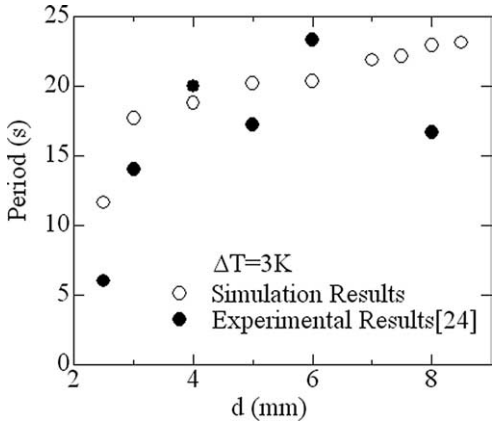

Fig. 8. Comparison between simulations and experiments on the oscillatory period.

reproduce the dip in the periods experimentally observed at $d = 8$ mm.

4. Conclusions

A series of 2-D numerical simulations of the thermocapillary convections in annular pools of silicon oil with $Pr = 6.7$

were conducted by means of the finite volume method. The results showed time-dependent convection is possible if A exceeds a critical value A_{cri} which is around 2.29. Hopf bifurcation neutral curve is delineated in the thermocapillary Reynolds number—aspect ratio plane. For the shallow layer, the flow cells originate near the inner cylinder, travel along the radial direction and merge into the stable strong cell near the outer cylinder. These moving cells are similar with the hydrothermal wave. In the deep pool, only one strong cell extends and contracts along the radial direction. Good agreements on oscillatory frequency and period were found between the simulation results and the experimental ones of Schwabe and Benz [24,25].

References

[1] D.T.J. Hurle, Thermo-hydrodynamic oscillation in liquid metals: The cause of impurities striations in melt-grown crystals, J. Phys. Chem. Solids 1 (1967) 659–669.

[2] H.G. Levich, V.S. Krylov, Surface tension-driven phenomena, Annual Rev. Fluid Mech. 1 (1969) 293–316.

[3] S. Ostrach, Low-gravity fluid flows, Annual Rev. Fluid Mech. 14 (1982) 313–345.

[4] S.H. Davis, Thermocapillary instabilities, Annual Rev. Fluid Mech. 19 (1987) 403–435.

[5] H. Ben Hadid, B. Roux, Buoyancy and thermocapillary-driven flows in shallow open cavity unsteady flow regimes, J. Crystal Growth 97 (1989) 217–225.

[6] H. Ben Hadid, B. Roux, Thermocapillary convection in long horizontal layers of low-Prandtl-number melts subject to a horizontal temperature gradient, J. Fluid Mech. 221 (1990) 77–103.

[7] H. Ben Hadid, B. Roux, Buoyancy- and thermocapillary-driven flows in differentially heated cavities for low-Prandtl-number fluids, J. Fluid Mech. 235 (1992) 1–36.

[8] D. Villers, J.K. Platten, Coupled buoyancy and Marangoni convection in acetone: Experiments and comparison with numerical simulations, J. Fluid Mech. 234 (1992) 487–510.

[9] L.J. Peltier, S. Biringen, Time-dependent thermocapillary convection in a rectangular cavity: Numerical results for a moderate Prandtl number fluid, J. Fluid Mech. 257 (1990) 339–357.

[10] J. Xu, A. Zebib, Oscillatory two- and three-dimensional thermocapillary convection, J. Fluid Mech. 364 (1998) 187–209.

[11] F. Daviaud, J.M. Vince, Traveling waves in a fluid layer subjected to a horizontal temperature gradient, Phys. Rev. E 48 (1993) 4432–4436.

[12] M.G. Braunsfurth, G.M. Homsy, Combined thermocapillary-buoyancy convection in a cavity. Part II. An experimental study, Phys. Fluids 9 (1997) 1277–1286.

[13] A. Garcimartin, N. Mukolobwiez, F. Daviaud, Origin of waves in surface–tension–driven convection, Phys. Rev. E 56 (1997) 1699–1705.

[14] R.J. Riley, G.P. Neitzel, Instability of thermocapillary-buoyancy convection in shallow layers. Part 1. Characterization of steady and oscillatory instabilities, J. Fluid Mech. 359 (1998) 143–164.

[15] S. Benz, P. Hintz, R.J. Riley, G.P. Neitzel, Instability of thermocapillary-buoyancy convection in shallow layers. Part 2. Suppression of hydrothermal waves, J. Fluid Mech. 359 (1998) 165–180.

[16] M.A. Pelacho, J. Burguete, Temperature oscillations of hydrothermal waves in thermocapillary-buoyancy convection, Phys. Rev. E 59 (1999) 835–840.

[17] M.A. Pelacho, A. Garcimartin, J. Burguete, Local Marangoni number at the onset of hydrothermal waves, Phys. Rev. E 62 (2000) 477–483.

[18] J. Burguete, N. Mukolobwiez, F. Daviaud, N. Garnier, A. Chiffaudel, Buoyant-thermocapillary instabilities in extended liquid layers subjected to a horizontal temperature gradient, Phys. Fluids 13 (2001) 2773–2787.

[19] A.B. Ezersky, A. Garcimartin, J. Burguete, H.L. Mancini, C. Perez-Garcia, Hydrothermal waves in Marangoni convection in a cylindrical container, Phys. Rev. E 47 (1993) 1126–1131.

[20] N. Mukolobwiez, A. Chiffaudel, F. Daviaud, Supercritical Eckhaus instability for surface–tension–driven hydrothermal waves, Phys. Rev. Lett. 80 (1998) 4661–4664.

[21] N. Garnier, A. Chiffaudel, Two dimensional hydrothermal waves in an extended cylindrical vessel, European Phys. J. B 19 (2001) 87–95.

[22] T. Azami, S. Nakamura, M. Eguchi, T. Hibiya, The role of surface–tension–driven flow in the formation of a surface pattern on a Czochralski silicon melt, J. Crystal Growth 233 (2001) 99–107.

[23] M.K. Smith, S.H. Davis, Instabilities of dynamic thermocapillary liquid layers. Part 1. Convective instabilities, J. Fluid Mech. 132 (1983) 119–144.

[24] D. Schwabe, S. Benz, Thermocapillary flow instabilities in an annulus under microgravity—results of the experiment MAGIA, Adv. Space Res. 29 (2002) 629–638.

[25] D. Schwabe, A. Zebib, B.C. Sim, Oscillatory thermocapillary convection in open cylindrical annuli. Part 1. Experiments under microgravity, J. Fluid Mech. 491 (2003) 239–258.

[26] Y.R. Li, L. Peng, Y. Akiyama, N. Imaishi, Three-dimensional numerical simulation of thermocapillary flow of moderate Prandtl number fluid in an annular pool, J. Crystal Growth 259 (2003) 374–387.